1D Coordination Polymer $(OPD)_2Co^{II}SO_4$ Revealing SMM Behaviour and Multiple Relaxation Modes

Piotr Konieczny,[a*] Anabel B. Gonzalez-Guillén, [b] Katarzyna Luberda-Durnaś,[c] Erik Čižmár,[d] Robert Pełka,[a] Marcin Oszajca,[b] Wiesław Łasocha[b,e]

[a]*Institute of Nuclear Physics PAN, Radzikowskiego 152, 31-342 Kraków, Poland (4812) 662 8019. E-mail: piotr.konieczny@ifj.edu.pl*

[b] *Faculty of Chemistry, Jagiellonian University, Gronostajowa 2, 30-387 Kraków, Poland*

[c] *Institute of Geological Sciences PAS, Research Centre in Kraków, Senacka 1, 31-002 Kraków, Poland*

[d] *Institute of Physics, Faculty of Science, Pavol Jozef Šafárik University, Park Angelinum 9, 04154 Košice, Slovakia*

[e] *Jerzy Haber Institute of Catalysis and Surface Chemistry PAS, Niezapominajek 8, 30-239 Krakow, Poland*

Table S1. Crystallographic data, Details of data collection, and structure refinement parameters for compound**1**.

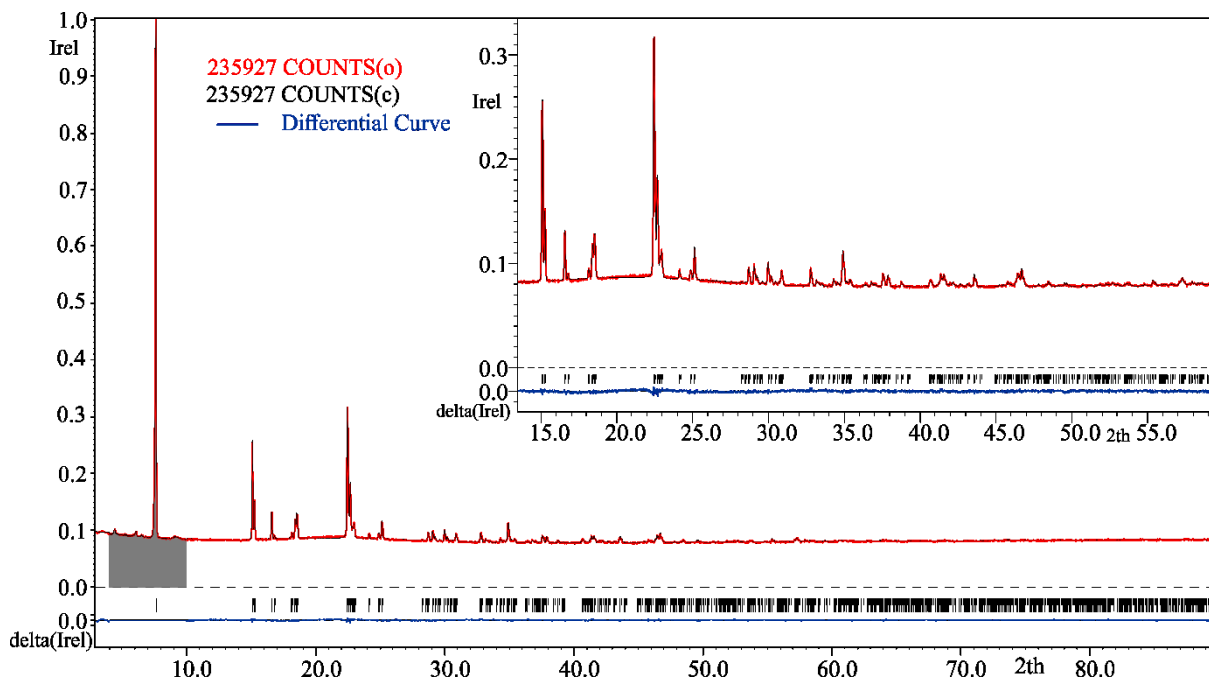| Compound	1
Source	Laboratory X-ray
Wavelenght	Cu Kα (1.54178 Å)
formula	$CoSO_4C_{12}H_{16}N_4$
Temperature / K	293
Formula weight / $g \cdot mol^{-1}$	371.3
Crystal system	Monoclinic
Space group No.	15 (I 1 2/a 1)
a [Å]	23.2051(19)
b [Å]	6.0605(3)
c [Å]	10.6819(6)
β [°]	90.924(6)
V [Å³]	1502.06(17)
Z	4
Pattern range 2θ [°]	3.016 - 89.986
Number of points (N)	6691
Number of parameters (P)	59
Number of restraints	28
$X^{2\,a}$	1.59
Rp [%][b]	0.76
Rwp [%][c]	1.12
a)$X^2=[\sum w(Io - Ic)^2/(N - P)]^{1/2}$. b) $Rp=\sum|Io - Ic|/\sum Io$. c) $Rwp=[\sum w(Io - Ic)^2/\sum wIo^2]^{1/2}$.	

Figure S1. Rietveld plot of compounds **1**.at room temperature: experimental data, red line; calculated profile, black line; allowed Bragg reflections, vertical marks. The difference between the experimental and calculated profiles is displayed as a blue continuous line. The inset shows an enlarged view from 15-60 2θ; gray section, reflection (200) excluded from calculation to improve the stability of the refinement.
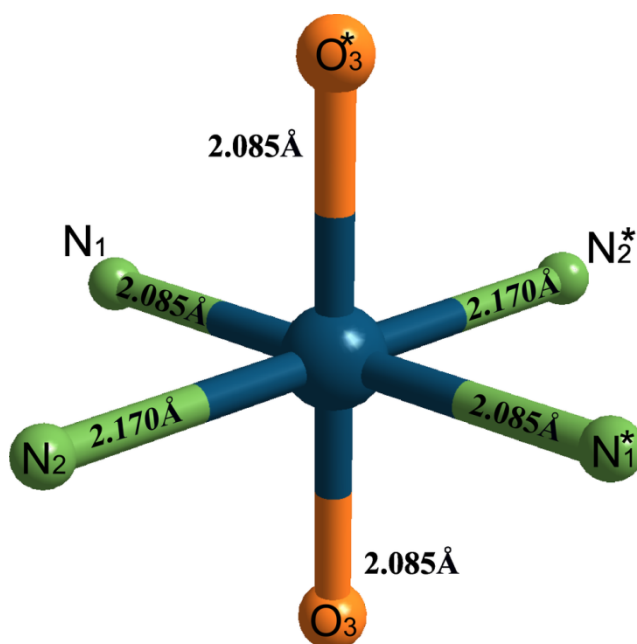

Figure S2. Coordination octahedron of the Co^{II} ion with bond lengths.

2

Table S2. Detailed structure parameters for **1**.

bond / Å or angle / deg	1
Co-O3	2.084(15)
Co-O3[a]	2.084(15)
Co-N2	2.175(19)
Co-N2[a]	2.175(19)
Co-N1	2.27(2)
Co-N1[a]	2.27(2)
S1-O4	1.434(17)
S1-O4[a]	1.434(17)
S1-O3	1.434(17)
S1-O3[a]	1.434(17)
C8-C4	1.39(4)
C8-C7	1.39(3)
N2-C2	1.45(2)
C2-C5	1.39(2)
C2-C6	1.39(2)
N1-C6	1.45(2)
C4-C5	1.39(3)
C6-C7	1.39(3)
O3-Co-O3[a]	180.0(5)
O3-Co-N2	90.5(7)
O3-Co-N2[a]	89.5(7)
O3-Co-N1	90.5(7)
O3-Co-N1[a]	89.5(7)
O3 [a]-Co-N2	89.5(7)
O3[a]-Co-N2[a]	90.5(7)
O3[a]-Co-N1	89.5(7)
O3[a]-Co-N1[a]	90.5(7)
N2-Co-N2[a]	180.0(5)
N2-Co-N1	79.5(8)
N2-Co-N1[a]	100.5(8)
N2[a]-Co-N1	100.5(8)
N2[a]-Co-N1[a]	79.5(8)
N1-Co-N1[a]	180.0(5)
O4-S1-O4[b]	109.5(12)
O4-S1-O3	109.5(10)
O4-S1-O3[b]	109.5(10)
O4[b]-S1-O3	109.5(10)
O4[b]-S1-O3[b]	109.5(10)
O3-S1-O3 [b]	109.5(11)
C4-C8-C7	120.0(16)
N2-C2-C5	120.0(17)
N2-C2-C6	120.0(16)
C5-C2-C6	120.0(16)
C8-C4-C5	120.0(18)
C2-C5-C4	120.0(19)
C2-C5-N1	120.0(16)

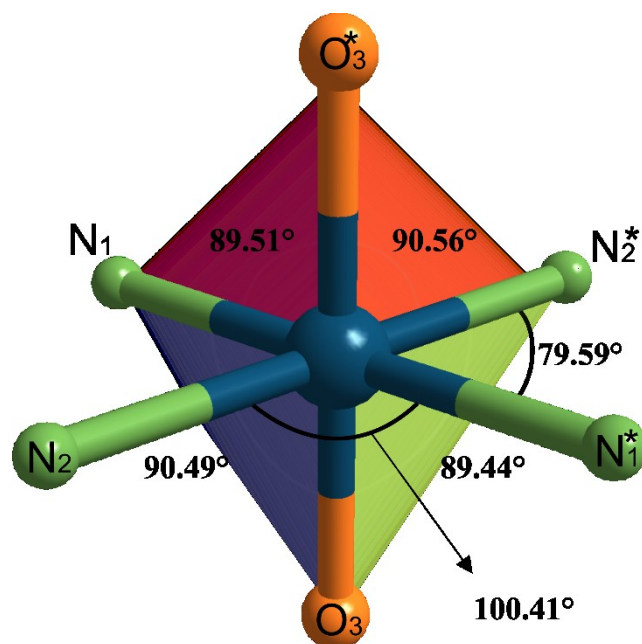| bond / Å or angle / deg	1
C2-C6-C7	120.0(15)
N1-C6-C7	120.0(17)
C8-C7-C6	120.0(18)
a) -x+1/2,-y+3/2,-z+1/2;	
b) -x+1/2,y,-z+1	

Figure S3. Coordination octahedron of the Co^{II} ion with angles.

Thermal stability of hybrid materials.. The first stage of amine removing can be split into two part (Figure S2 and S3). In first (**I**), only about 2-3 wt% of amine is removed up to 230ºC. Next (**II**), rapid amine remove, results in structure collapse and is observed in the temperature range 230-320ºC. In the final stage, both amine and SO_x/O_2 are removed. Similar behaviour is observed in both atmospheres.
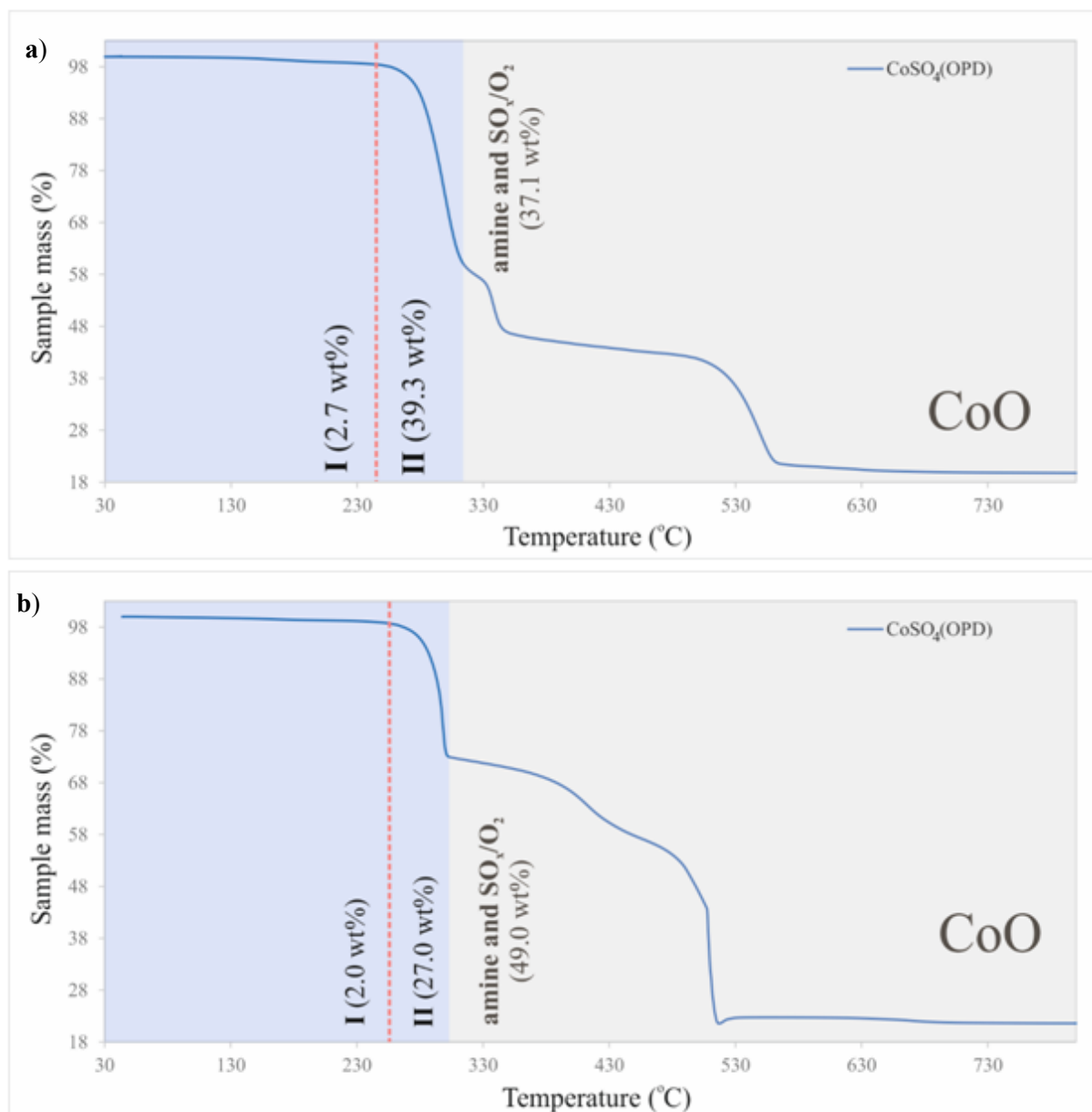

Figure S4. TG curves of sample **1** in (**a**) nitrogen and (**b**) air; heating rate 10ºC/min. The red-dashed line represents the border between rapid and slow amine removing. The two steps of thermal decompositions are shown by colours; blue-sole amine removing; grey- amine and SO_x/O_2 removing.
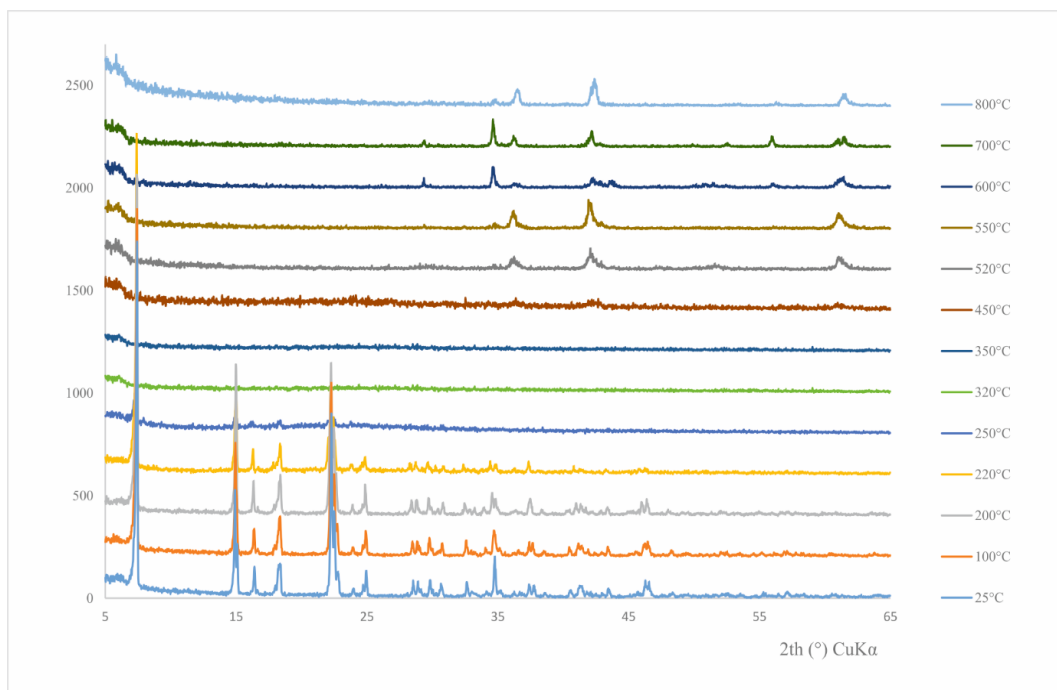
Figure S5. XRD patters of **1** at different temperatures in air; ramp rate 10°C/min. The following phases were found: hybrid material - 25-250°C; amorphous phase - 250-350°C; CoO (COD 9008618) - 450-800°C.
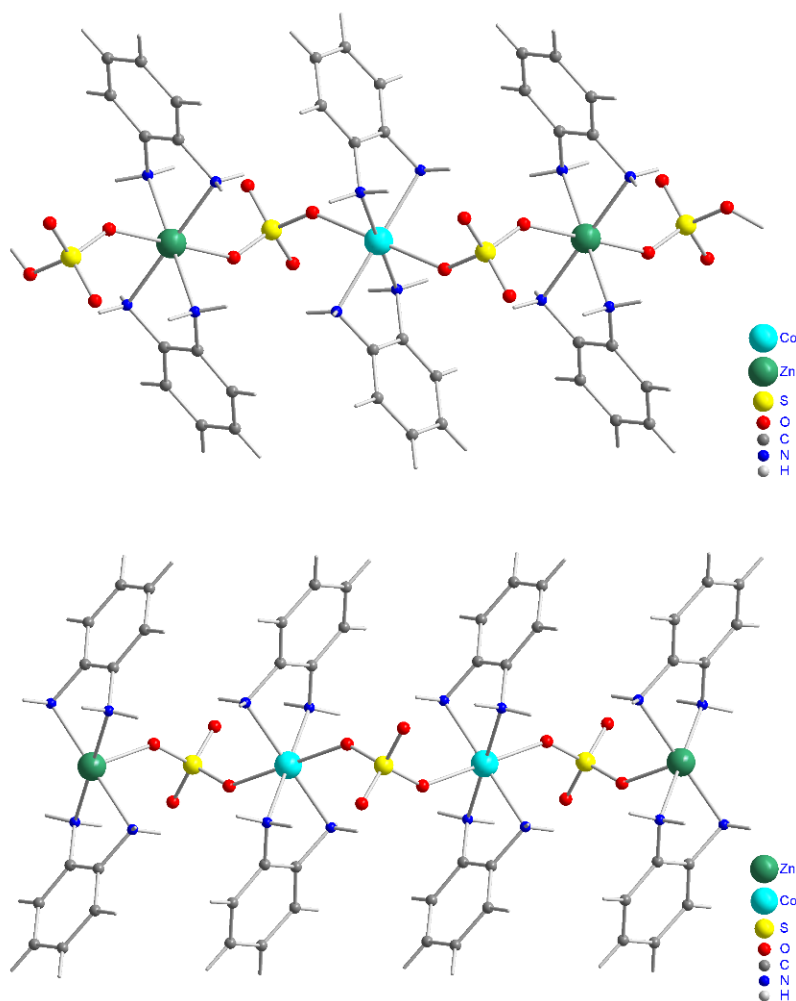
Figure S6. An example of the largest model fragments used for ab initio and BS DFT calculations plotted using Diamond software, **Fr5** – upper panel, **Fr8** – lower panel.

Table S3. Exchange coupling between two neighbouring Co^{II} ions obtained from the BS DFT calculations using B3LYP and TPSSh functionals for different model fragments.

model fragment	J_{BS} (cm^{-1}), B3LYP	J_{BS} (cm^{-1}), TPSSh
H-SO$_4$-Co(OPD)$_2$-SO$_4$-Co(OPD)$_2$-SO$_4$-H (**Fr6**)	-0.1	-0.27
Na-SO$_4$-Co(OPD)$_2$-SO$_4$-Co(OPD)$_2$-SO$_4$-Na (**Fr7**)	-0.03	-0.16
Zn(OPD)$_2$-SO$_4$-Co(OPD)$_2$-SO$_4$-Co(OPD)$_2$-SO$_4$-Zn(OPD)$_2$ (**Fr8**)	-0.06	-0.20

*An attempt to perform calculations on model fragments **Fr3** and **Fr8** omitting OPD ligand for terminal Zn^{II} ion yielded an unbalanced charge distribution in the model fragment and less accurate results. As a result, e.g., for the BS DFT calculation the inspection of the Mulliken spin population showed an overestimated spin delocalization with a value of 0.9 on terminal Zn^{II} ions yielding a ferromagnetic exchange interaction not evidenced by the experimental data.
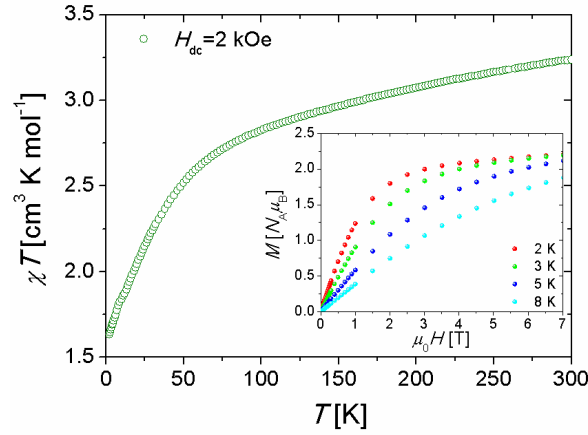
Figure S7. Temperature dependence of χT of the undiluted sample detected in H_{dc}=2 kOe. Inset: Field dependence of the isothermal magnetization of the undiluted sample detected at 2, 3, 5, and 8 K. No model calculations have been performed for these data as there is no simple way to account for the substantial intermolecular interactions.

Magnetization averaging with SOPHE spherical code

The DC magnetic properties of **1d** were calculated within the zero-field splitting (ZFS) Hamiltonian for the spin S=3/2 ion in a triaxial crystal field involving the anisotropic Zeeman term [1]. The powder sample susceptibility was calculated as the mean of three principal values of the susceptibility tensor $\bar{\chi} = 1/3(\chi_{xx} + \chi_{yy} + \chi_{zz})$. The averaging of the magnetization employed the SOPHE spherical code [2,3] involving 925 different field directions uniformly distributed over the upper hemisphere. The spherical angles (θ, φ) corresponding to the orientation knots read

$$\theta_j = \frac{j}{M}\frac{\pi}{2}, \quad j = 0,1,\ldots,M$$

$$\varphi_{jk} = \frac{k}{j}\frac{\pi}{2}, \quad k = 0,1,\ldots,4j-1$$

(S1)

where M(=21) specifies the number of knots along a quarter of a meridian. The total number of knots is $2M(M+1)+1$. Figure S8 shows the configuration of the orientations marked by red points together with the igloo-type partition of the solid angle associated with these orientations (blue lines). The weight factors corresponding to this particular partition read

$$w_{jk} = \begin{cases} \dfrac{1}{2j}\sin\left(\dfrac{j}{M}\dfrac{\pi}{2}\right)\sin\left(\dfrac{\pi}{4M}\right) & \text{for} \quad j \neq 0 \wedge j \neq M \\[2mm] 2\sin^2\left(\dfrac{\pi}{8M}\right) & \text{for} \quad j = 0 \\[2mm] \dfrac{1}{4M}\sin\left(\dfrac{\pi}{4M}\right) & \text{for} \quad j = M \end{cases}$$
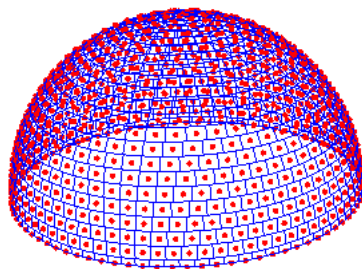
(S2)

Figure S8: Distribution of field orientations (red points) corresponding to the SOPHE spherical code. The blue lines show the igloo-like partition of the solid angle determining the values of the weight factors.

More dense angle grids took substantially longer times without yielding apparent differences in the calculated values. The corresponding procedures were implemented and carried out within the *Mathematica8.0* environment.
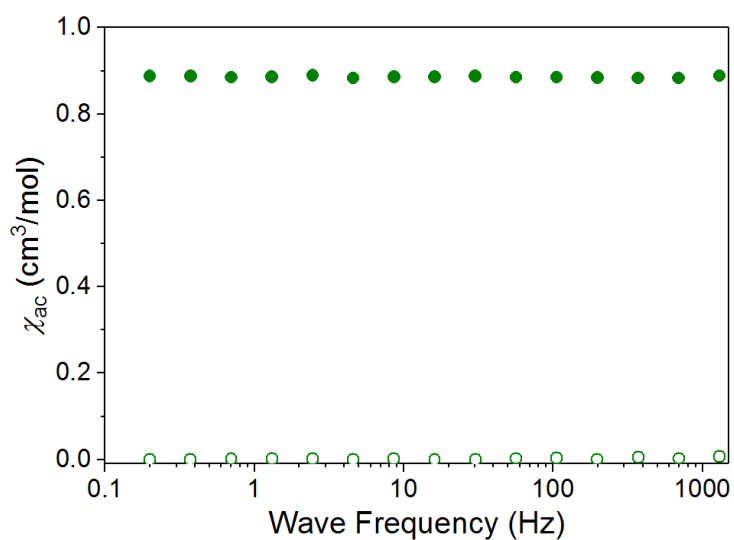

Figure S9. Frequency dependence of ac susceptibility of **1** at 2.0 K without external field.
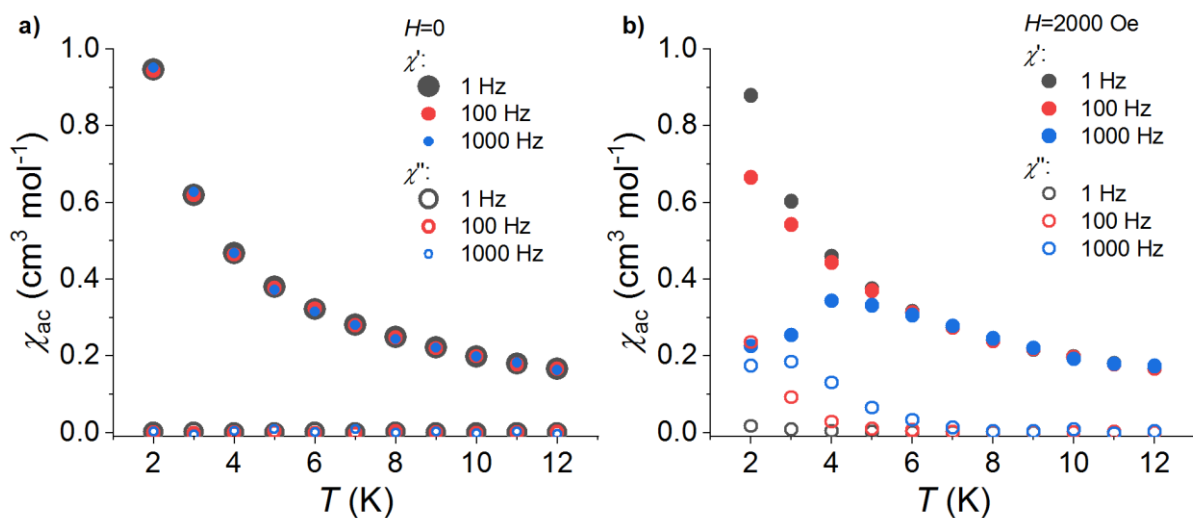
Figure S10. Temperature dependence of ac susceptibility without external magnetic field (a) and with applied field of 2000 Oe (b). The full circles stand for the in-phase component, whereas the empty circles represent the out-of-phase signal.
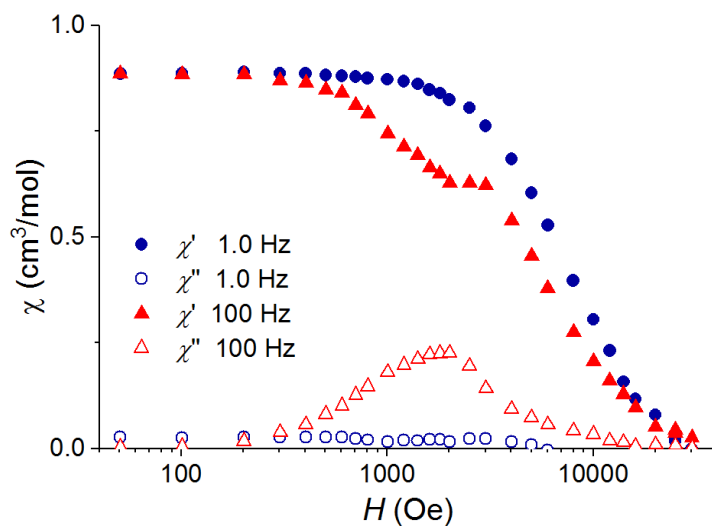
Figure S11. Field dependence of χ_{ac} at 2.0 K. In-phase component - full symbols, out-of-phase signal - empty symbols.
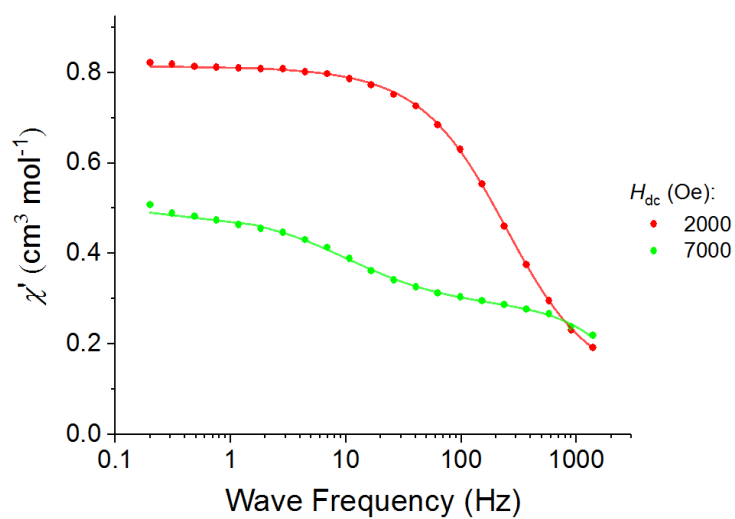
Figure S12.Frequency dependence of in-phase ac susceptibility (χ') under 2000 Oe and 7000 Oe dc field at 2.0 K.
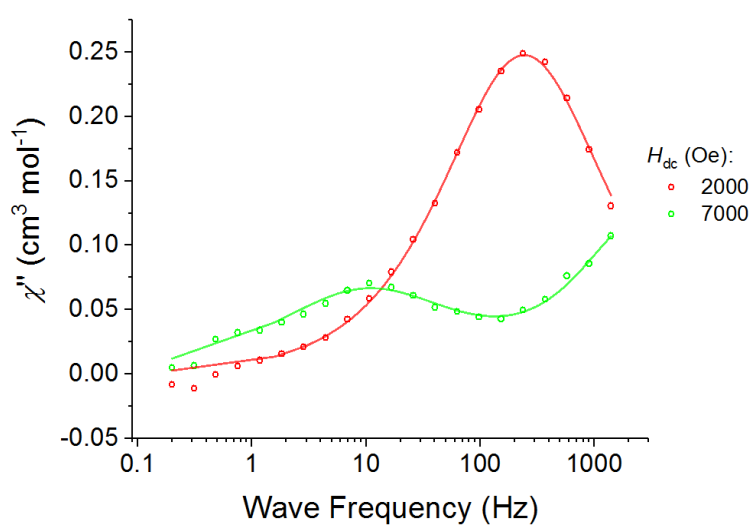
Figure S13. Frequency dependence of out-phase ac susceptibility (χ'') under 2000 Oe and 7000 Oe dc field at 2.0 K.

Analysis of relaxation processes

In order to analyze relaxations detected in the samples the extended Debye model was used accounting for two independent relaxation processes. The total ac susceptibility signal is in this model given by the formula

$$\chi_{\text{total}}(\omega) = \chi_S + (\chi_T - \chi_S)\left[\frac{\beta}{1+(i\omega\tau_1)^{1-\alpha_1}} + \frac{1-\beta}{1+(i\omega\tau_2)^{1-\alpha_2}}\right], \quad \text{(S3)}$$

where χ_S is the adiabatic susceptibility, χ_T is the isothermal susceptibility, $\omega=2\pi f$ is the angular frequency, τ_1 and τ_2 are the magnetization relaxation times, α_1 and α_2 describe the distributions of the relaxation processes, β is the weight of the first relaxation process and $1-\beta$ corresponds to the second one. The real part and the imaginary part are given by Eq. (S4) and Eq. (S5), respectively.

$$\chi' = \chi_S + (\chi_T - \chi_S) \times$$
$$\left\{\frac{\beta[1+(\omega\tau_1)^{1-\alpha_1}\sin(1/2\alpha_1\pi)]}{1+2(\omega\tau_1)^{1-\alpha_1}\sin(1/2\alpha_1\pi)+(\omega\tau_1)^{2(1-\alpha_1)}} + \frac{(1-\beta)[1+(\omega\tau_2)^{1-\alpha_2}\sin(1/2\alpha_2\pi)]}{1+2(\omega\tau_2)^{1-\alpha_2}\sin(1/2\alpha_2\pi)+(\omega\tau_2)^{2(1-\alpha_2)}}\right\} \quad \text{(S4)}$$

$$\chi'' = (\chi_T - \chi_S)\left\{\frac{\beta(\omega\tau_1)^{1-\alpha_1}\cos(1/2\alpha_1\pi)}{1+2(\omega\tau_1)^{1-\alpha_1}\sin(1/2\alpha_1\pi)+(\omega\tau_1)^{2(1-\alpha_1)}} + \frac{(1-\beta)(\omega\tau_2)^{1-\alpha_2}\cos(1/2\alpha_2\pi)}{1+2(\omega\tau_2)^{1-\alpha_2}\sin(1/2\alpha_2\pi)+(\omega\tau_2)^{2(1-\alpha_2)}}\right\}$$
$$\text{(S5)}$$

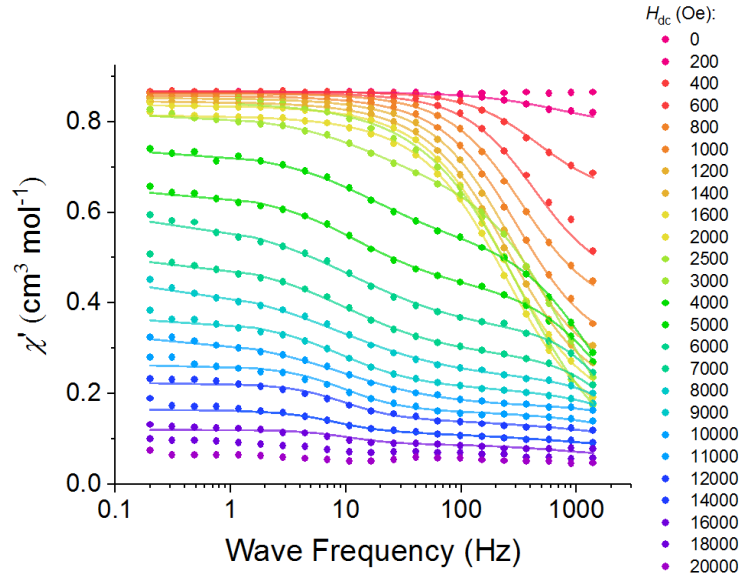The experimental data of χ' and χ'' were fitted simultaneously.

Figure S14. Frequency dependence of in-phase ac susceptibility (χ') in dc field range: 0 - 20000 Oe at 2.0 K. The solid lines correspond to the extended Debye model fits.
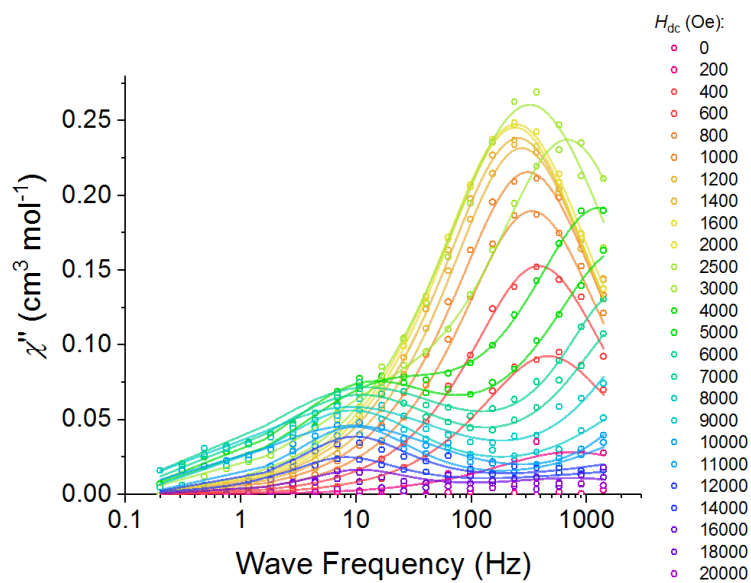
Figure S15. Frequency dependence of out-of-phase ac susceptibility (χ'') in dc field range: 0 - 20000 Oe at 2.0 K. The solid lines correspondto the extended Debye model fits.
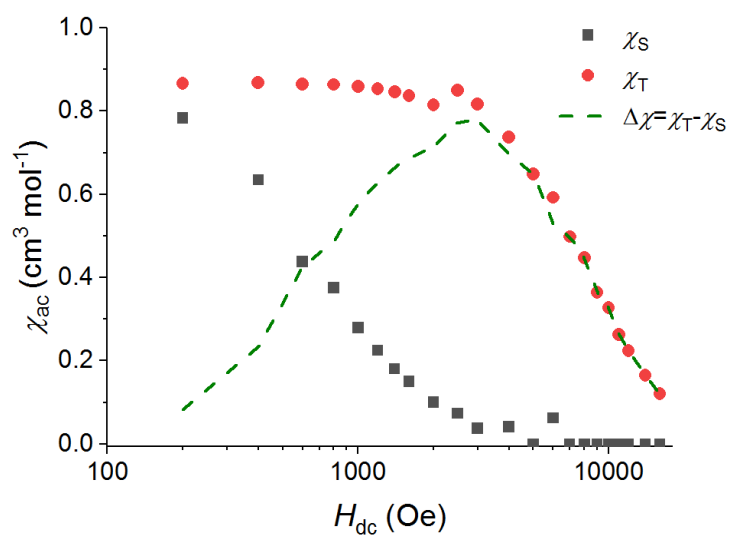

Figurre S16. Dc field dependence of the adiabatic susceptibility χ_S (black squares), isothermal susceptibility χ_T (red circles) and its difference $\Delta\chi = \chi_T - \chi_S$ (green dashed line) at 2.0 K.
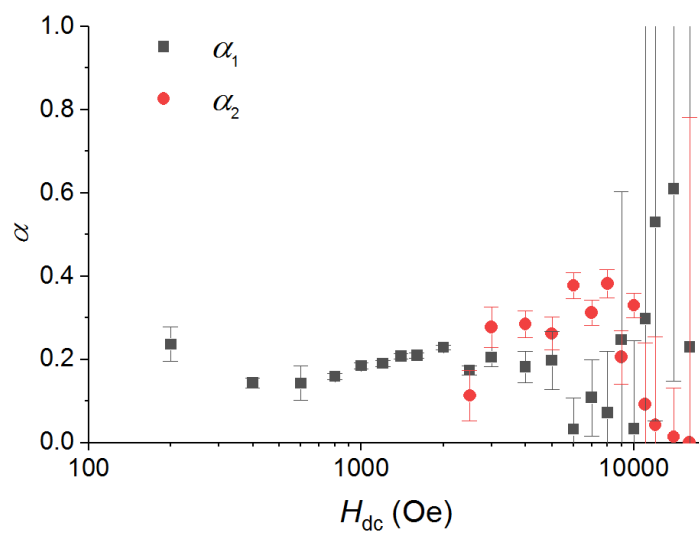
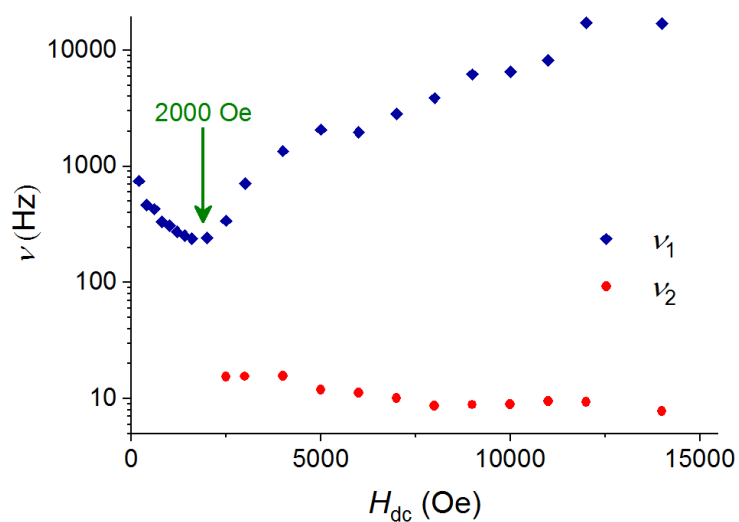**Figure S17**.Dc field dependence of α_1 and α_2 parameters at 2.0 K.

Figure S18. Dc field dependence of relaxation rate $1/\tau_1=\nu_1$ (blue diamonds) and $1/\tau_2=\nu_2$ (red circles) at 2.0 K. The minimum of ν_1 is marked with green arrow.
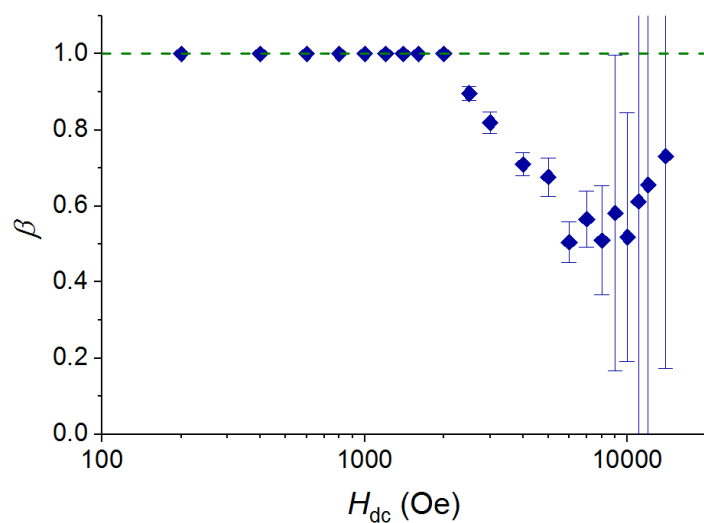
Figure S19. Dc field dependence of the weight of the first relaxation process β at 2.0 K.
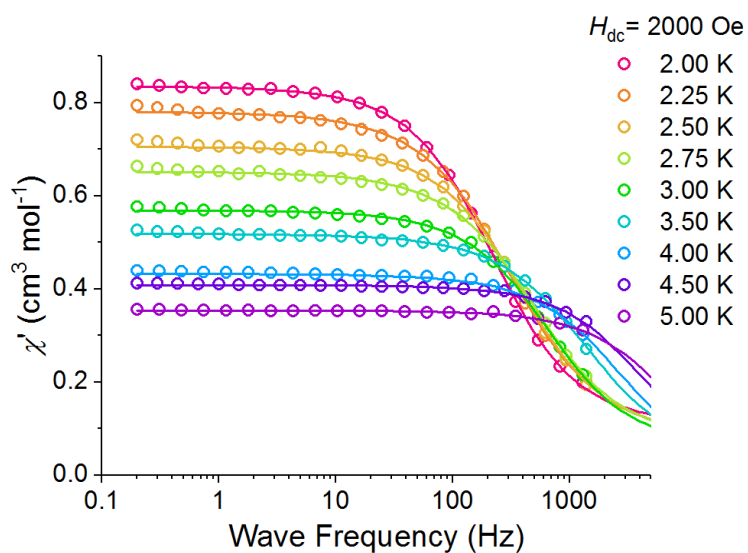
Figure S20. Frequency dependence of in-phase ac susceptibility (χ') with applied field 2000 Oe in temperature range: 2.0 K - 5.0 K. The solid lines correspondto the extended Debye model fits.
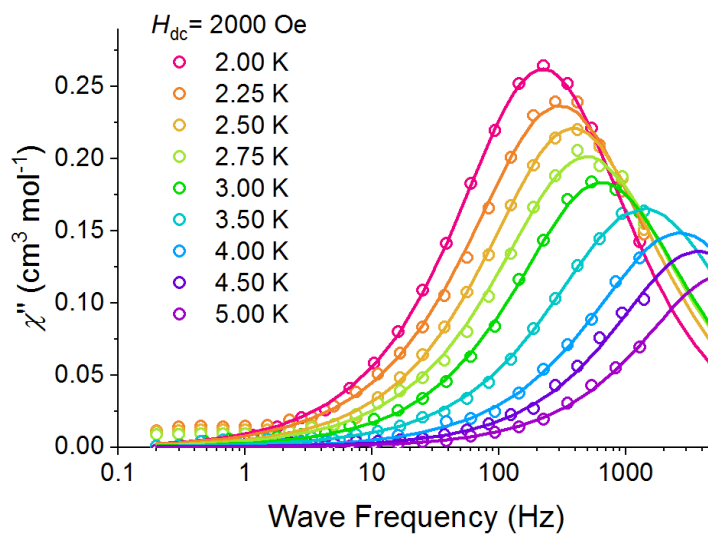
Figure S21. Frequency dependence of out-of-phase ac susceptibility (χ'') with applied field 2000 Oe in temperature range: 2.0 K - 5.0 K. The solid lines correspondto the extended Debye model fits.
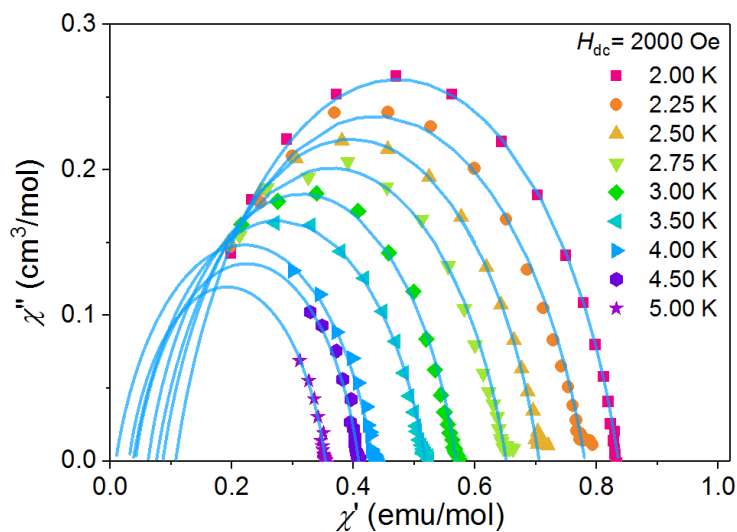
Figure S22.Cole-Cole plots corresponding to the ac susceptibilities detected for compound **1** in the applied field of 2000 Oe and temperature range: 2.0-5.0 K. Solid lines show the best fits to the extended Debye model.
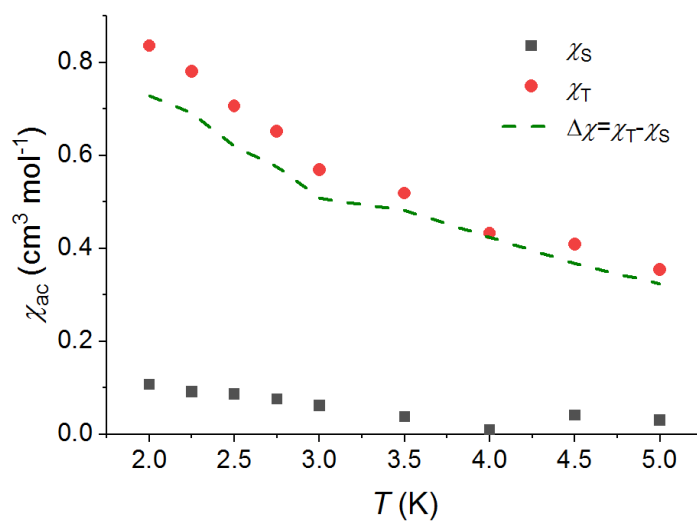
Figure S23. Temperature dependence of the adiabatic susceptibility χ_S (black squares), isothermal susceptibility χ_T (red circles) and its difference $\Delta\chi=\chi_T-\chi_S$ (green dashed line) at 2000 Oe dc field.
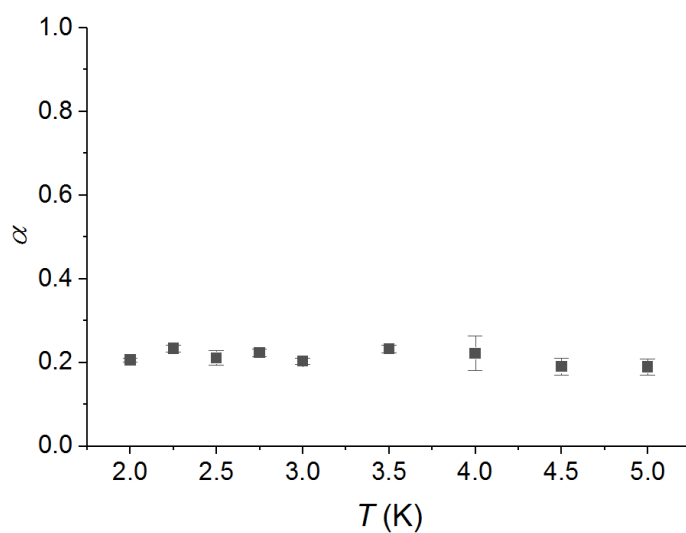
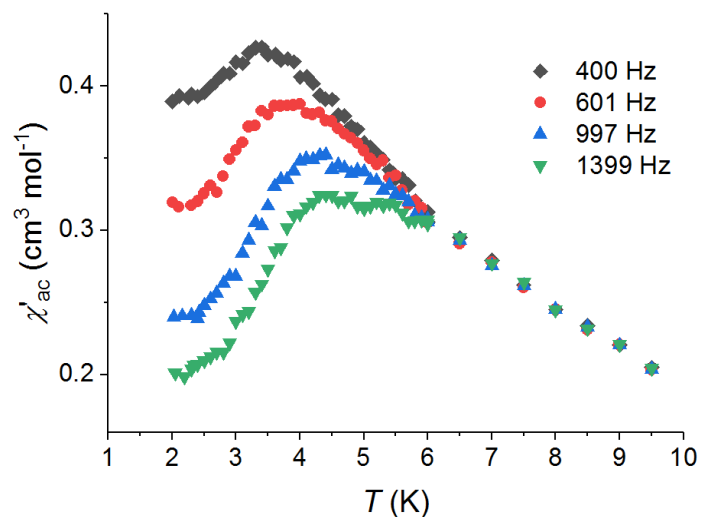**Figure S24**.Temperature dependence of α_1 parameter at 2000 Oe.

Figure S25. Temperature dependence of χ_{ac} in-phase component with applied field 2000 Oe. These results were used to calculate the Mydosh parameter.
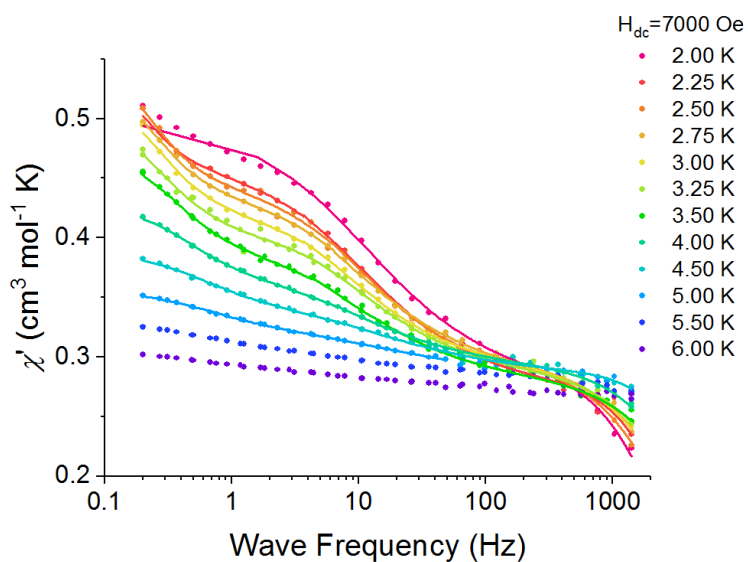

Figure S26. Frequency dependence of in-phase ac susceptibility (χ') with applied field 7000 Oe in the temperature range: 2.0 K - 6.0 K. The solid lines correspondto the extended Debye model fits.
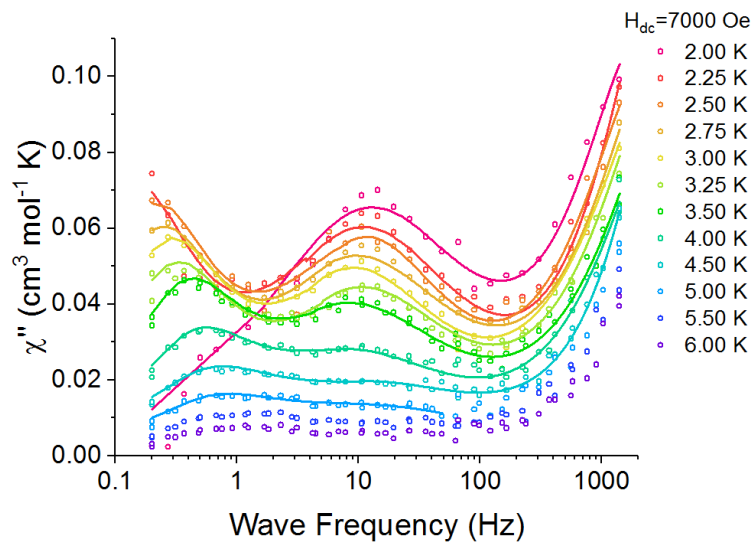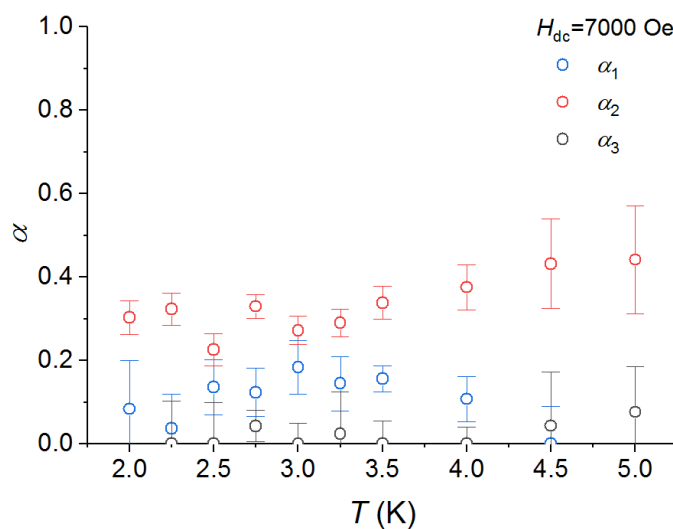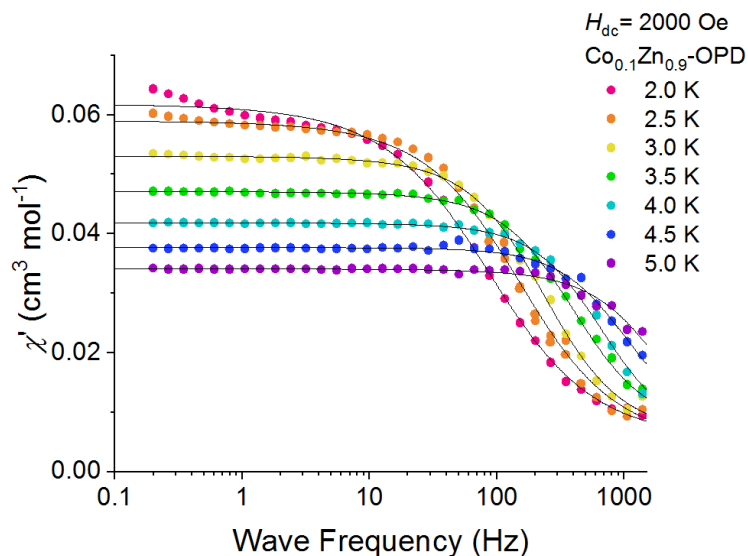
Figure S27. Frequency dependence of out-of-phase ac susceptibility (χ'') with applied field 7000 Oe in temperature range: 2.0 K - 6.0 K. The solid lines correspond to the extended Debye model fits.

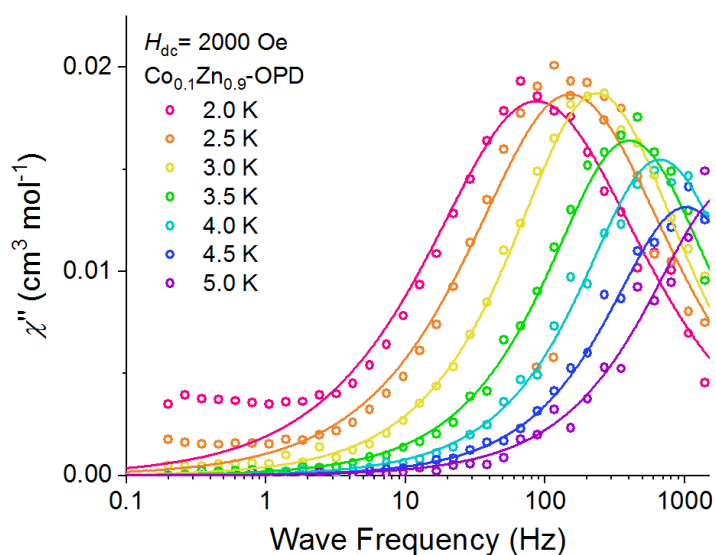**Figure S28**. Temperature dependence of α_1, α_2 and α_3 parameters at 7000 Oe.

Figure S29. Frequency dependence of in-phase ac susceptibility (χ') with applied field 2000 Oe in temperature range: 2.0 K - 5.0 K for the diluted compound $Co_{0.1}Zn_{0.9}$-OPD. The solid lines correspond to the extended Debye model fits.

Figure S30. Frequency dependence of out-of-phase ac susceptibility (χ'') with applied field 2000 Oe in temperature range: 2.0 K - 5.0 K for the diluted compound $Co_{0.1}Zn_{0.9}$-OPD. The solid lines correspond to the extended Debye model fits.

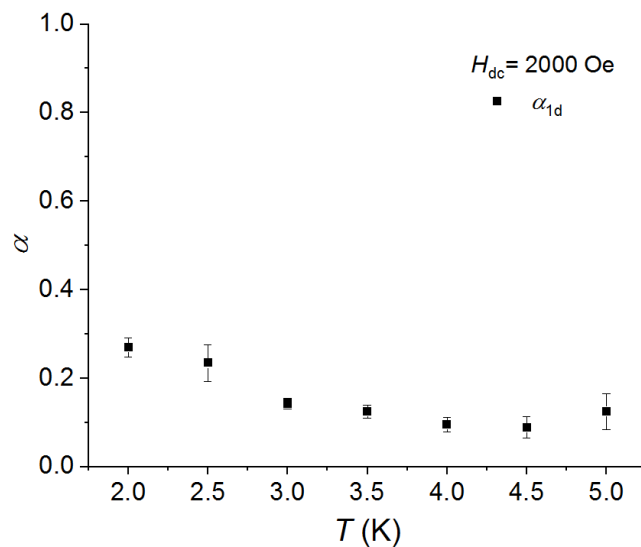**Figure S31**. Temperature dependence of α_{1d} parameter at 2000 Oe for the diluted compound $Co_{0.1}Zn_{0.9}$-OPD.
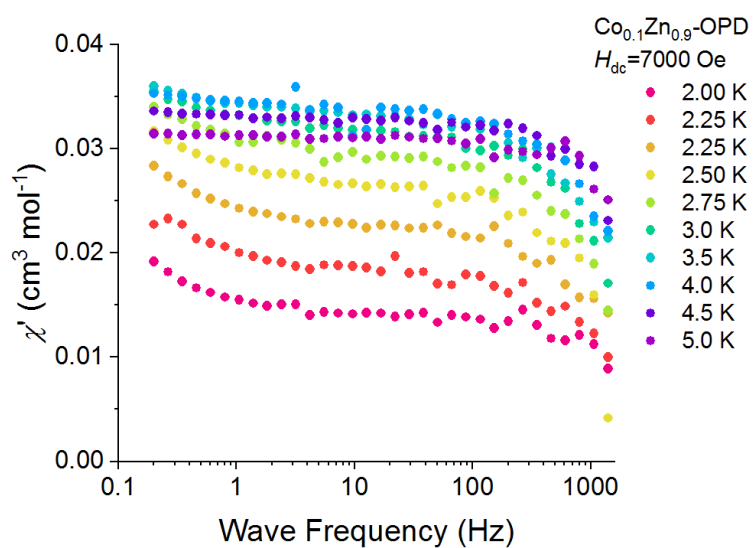

Figure S32. Frequency dependence of in-phase ac susceptibility (χ') with applied field 7000 Oe in temperature range: 2.0 K - 5.0 K for the diluted compound $Co_{0.1}Zn_{0.9}$-OPD.
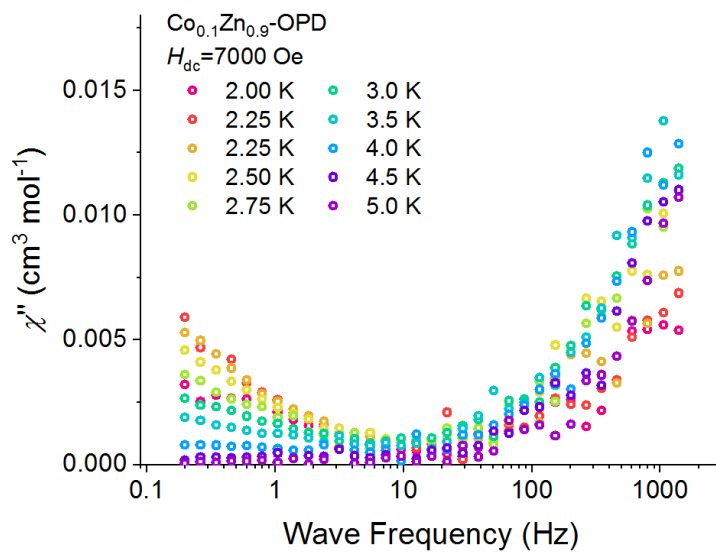
Figure S33. Frequency dependence of out-of-phase ac susceptibility (χ'') with applied field 7000 Oe in temperature range: 2.0 K - 5.0 K for the diluted compound $Co_{0.1}Zn_{0.9}$-OPD.

References

[1] O. Kahn, *Molecular Magnetism*, VCH Publishers, Inc.: Weinheim, Germany, 1993.

[2] D. Wang, G. R. Hanson, *J. Magn. Res. A***117** (1995) 1-8.

[3] A. Ponti, *J. Magn. Res.* **138** (1999) 288-297.